Chinese Chemical Letters 33 (2022) 1403–1406

Contents lists available at ScienceDirect

Chinese Chemical Letters

journal homepage: www.elsevier.com/locate/cclet

Robust hydrogen production from HCOOH over amino-modified KIT-6-confined PdIr alloy nanoparticles

Wenfang Peng[a,b], Shiwen Liu[b], Xiugang Li[a], Gang Feng[c], Jianhui Xia[a], Zhang-Hui Lu[a,*]

[a] Key Laboratory of Functional Small Molecules for Ministry of Education, College of Chemistry and Chemical Engineering, Jiangxi Normal University, Nanchang 330022, China
[b] Jiangxi Provincial Center for Disease Control and Prevention, Nanchang 330029, China
[c] College of Chemistry, Nanchang University, Nanchang 330031, China

ARTICLE INFO

Article history:
Received 29 June 2021
Revised 31 July 2021
Accepted 9 August 2021
Available online 12 August 2021

Keywords:
Formic acid
Hydrogen production
Palladium
Metal nanoparticle
3D mesoporous silica

ABSTRACT

Formic acid (FA), which can be produced *via* CO_2 reduction and biomass conversion, has received extensive interest as a convenient and safe hydrogen carrier due to its wide range of sources, renewable, high hydrogen content (4.4 wt%), and convenient storage/transportation. Designing highly efficient catalysts is the main challenge to realize the hydrogen production from FA. In this work, well-dispersed and electron-rich PdIr alloy nanoparticles with a size of 1.8 nm are confined in amino-modified 3D mesoporous silica KIT-6 and applied as a highly efficient catalyst for robust hydrogen production from FA at ambient temperature. Small PdIr alloy nanoparticles confined by amino-modified KIT-6 (PdIr/KIT-6-NH_2) lead to better catalytic activity compared to that of Pd/KIT-6-NH_2 and PdIr confined by bare KIT-6, achieving a high turnover frequency (TOF) value of 3533 h^{-1} at ambient temperature (303 K), 100% H_2 selectivity and conversion toward the dehydrogenation of FA, which is comparable to the best heterogeneous catalysts ever reported. The high catalytic activity of PdIr/KIT-6-NH_2 can be attributed to the synergistic effect between Pd and Ir, strong interaction between PdIr and KIT-6-NH_2, as well as the amino-groups of KIT-6-NH_2 which can act as a proton scavenger to promote the breaking of O-H bond of formic acid.

Hydrogen (H_2) is regarded as the most promising energy carrier to replace traditional fossil fuels in the future due to its high energy density, cleanliness, and renewability [1–4]. However, efficient and safe hydrogen storage technology is still a critical problem that needs to be solved. Formic acid (FA), which can be produced *via* CO_2 reduction and biomass conversion, has received extensive interest as a convenient and safe hydrogen carrier due to its wide range of sources, renewable, high hydrogen content (4.4 wt%), and convenient storage/transportation [5,6]. Formic acid can be selectively decomposed by dehydrogenation procedure ($HCOOH \rightarrow H_2 + CO_2$) or *via* a dehydration pathway ($HCOOH \rightarrow H_2O + CO$). The latter approach should be avoided because the generated CO is toxic to the fuel cells. Recently, a variety of efficient catalysts including the homogeneous and heterogeneous catalysts have been developed toward the hydrogen evolution from the FA dehydrogenation reaction (FDR). Heterogeneous catalysts have attracted much attention due to their advantages of being easily separated and recovered from reaction mixtures [7–9]. Pd-containing catalysts [10–19], especially PdAg [14–16] and AuPd [17–19] bimetallic catalysts, were found to be very active toward FDR.

Confining the active metal nanoparticles (NPs) in the matrix with large surface area would be an efficient method toward enhancing the catalytic activity of catalysts [20–29]. To date, several efficient supporting materials have been applied in FDR, such as graphene oxide [30,31], porous carbon [32,33], and metal-organic frameworks [34–36]. The supported Pd-containing catalysts showed the enhanced activity toward FDR; however, it remains a challenge to improve the catalytic performance toward the actual application in future. Mesoporous materials with high thermal and chemical stabilities have been widely used in adsorption, separation and catalysis [37–41], owing to their high specific surface area and regular pore structure. In addition, amine groups-modified mesoporous support can provide the anchoring sites for metal species to achieve small metal NPs, leading to the enhanced catalytic performance [42–45]. KIT-6 with 3D cubic structure as a carrier has more advantages in mass transfer and diffusion of reactive molecules, which can reduce hole blockage and provide more active sites. Due to its surface residual surface silicon (Si–OH), KIT-6 could be easily modified with amine groups, which can be used

* Corresponding author.
E-mail address: luzh@jxnu.edu.cn (Z.-H. Lu).

https://doi.org/10.1016/j.cclet.2021.08.033
1001-8417/

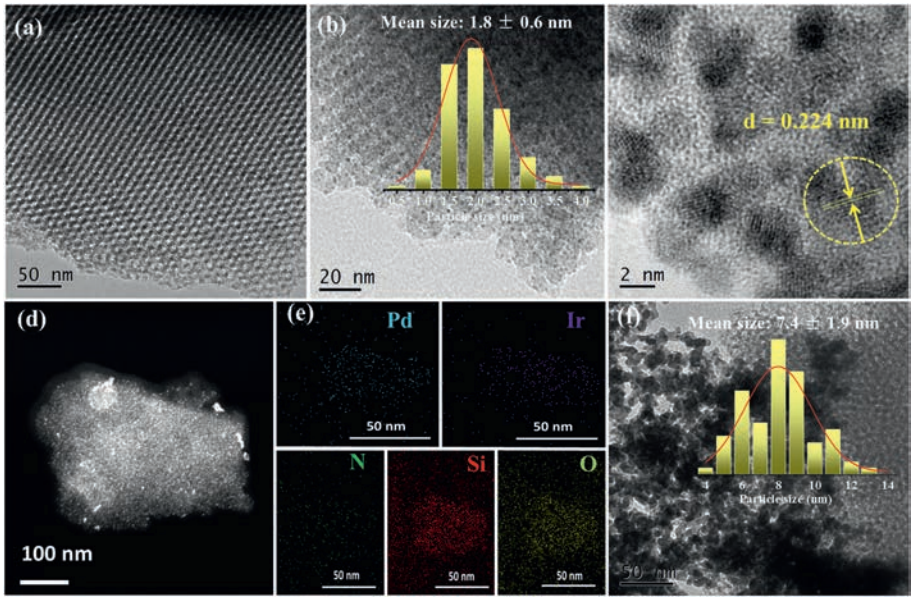

Fig. 1. (a) TEM of KIT-6-NH_2, (b) TEM, (c) HRTEM, (d) HAADF-STEM, (e) the corresponding EDS mapping of PdIr/KIT-6-NH_2 and (f) TEM of PdIr/KIT-6 (inset: the corresponding particle size histogram).

as the interaction site of metal NPs to obtain the ultrafine metal NPs as well as a proton scavenger to promote the breaking of O-H bond of FA.

Herein, small and highly dispersed PdIr alloy NPs with a mean particle size of 1.8 nm immobilized by amino-functionalized 3D mesoporous silica (KIT-6) were prepared by an impregnation-reduction approach and used as an efficient catalyst for FDR (see Supporting information for detailed experimental procedures). Benefiting from bimetallic synergy between Pd and Ir, strong interaction between small PdIr alloy NPs and KIT-6-NH_2, as well as the promotion of amino-groups of KIT-6-NH_2, the as-synthesized PdIr/KIT-6-NH_2 catalyst exhibits a superior activity toward FDR with a TOF value of 3533 h^{-1} at 303 K, which is comparable to the best heterogeneous catalysts ever reported [5–7,10–19,30–36].

As shown in Fig. 1, the typical transmission electron microscopy (TEM) images of KIT-6-NH_2 (Fig. 1a) and PdIr-KIT-6-NH_2 (Fig. 1b) display the ordered channel structure, similar as that of pure KIT-6 (Fig. S1 in Supporting information), confirmed by scanning electron microscopy (SEM) images (Figs. S1a and c). The Pd, Ir, N, Si and O elements were uniform dispersed in EDS elemental mappings (Figs. 1d and e). PdIr NPs with a mean size of about 1.8 nm were well dispersed in KIT-6-NH_2 (Fig. 1b). In contrast, larger and coagulated PdIr NPs with a mean size of 7.4 nm (Fig. 1f) were observed in bare KIT-6 without amino-group. It is clearly demonstrated that amino-groups of KIT-6-NH_2 result in the formation of smaller NPs due to the fact that amino-groups can effectively anchor the metal NPs and prevent them from aggregation. The amine-groups of KIT-6-NH_2 could be verified by Fourier transform infrared (FT-IR) spectra (Fig. S2 in Supporting information). The lattice spacing of the PdIr NPs of 0.224 nm (Fig. 1c) shows the formation of PdIr alloy structure in KIT-6-NH_2, which is between the (111) planes of face-centered cubic Ir (0.222 nm) and Pd (0.229 nm). The alloy structure of PdIr NPs was also confirmed by XRD results (Fig. S3 in Supporting information), in which a wide peak between the characteristic peaks of Pd (111) and Ir (111) can be observed. After annealed in Ar atmosphere at 873 K for 4 h (Fig. S4 in Supporting information), the alloy structure of PdIr NPs could be clearly observed.

As shown in Fig. 2a, the N_2 adsorption-desorption curves of the KIT-6, KIT-6-NH_2 and PdIr/KIT-6-NH_2 samples are of type IV curves, which is indicative of the ordered mesoporous materials and consistent with their TEM and small-angle XRD results (Fig. S3). As compared to KIT-6, the decrease in BET specific surface area, pore diameter, and pore volume of PdIr/KIT-6-NH_2 (Fig. 2a, Fig. S5 and Table S1 in Supporting information) can be owing to the amino-modification and metal NPs loading.

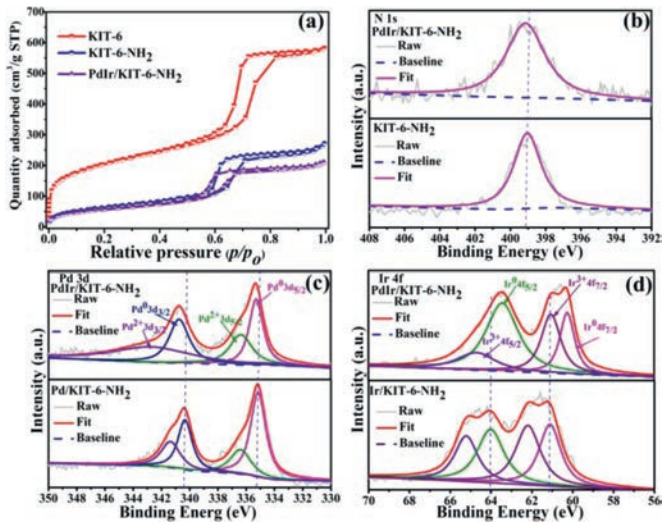

Fig. 2. (a) Nitrogen sorption isotherms of KIT-6, KIT-6-NH_2, and PdIr/KIT-6-NH_2, high-resolution XPS spectra of (b) N 1s in PdIr/KIT-6-NH_2 and KIT-6-NH_2, (c) Pd 3d in PdIr/KIT-6-NH_2 and Pd/KIT-6-NH_2 and (d) Ir 4f in PdIr/KIT-6-NH_2 and Ir/KIT-6-NH_2.

The survey XPS spectrum of PdIr/KIT-6-NH_2 reveals the existence of Pd, Ir, N, Si and O elements (Fig. S6 in Supporting information). As shown in Fig. 2b, N 1s has a higher binding energy in PdIr/KIT-6-NH_2 than that in KIT-6-NH_2, indicating the -NH_2 group may provide some electrons to the PdIr alloy NPs, resulting in electron enrichment of metal NPs, and thus enhance the dehydrogenation rate toward FDA. Compared with the PdIr/KIT-6-NH_2 catalysts, the Pd 3d peaks of Pd/KIT-6-NH_2 are shifted to lower binding energies, and an opposite tendency is observed in the case of the Ir 4f peaks of Ir/KIT-6-NH_2 (Figs. 2c and d). This outcome is pos-

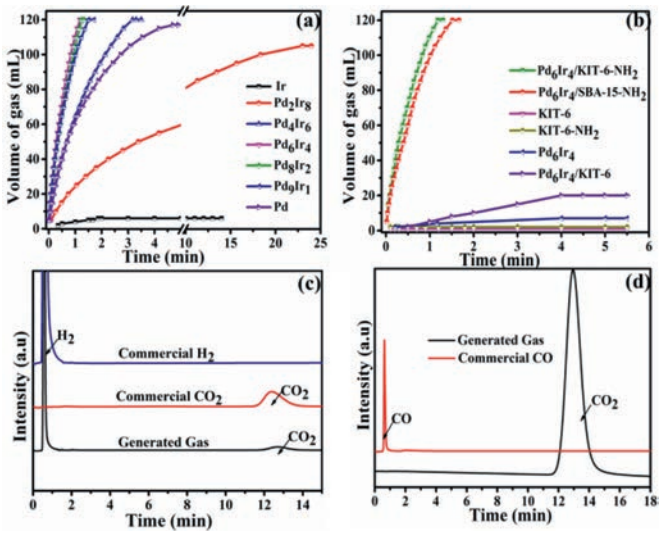

Fig. 3. Volume of the generated gas *versus* time for FDR in FA-SF aqueous solution over (a) Pd_xIr_{10-x}/KIT-6-NH_2 with different Pd/Ir ratios and (b) Pd_6Ir_4 NPs confined by different supports. GC spectra for the commercial gas and the generated gas from FDR over Pd_6Ir_4/KIT-6-NH_2 using (c) TCD detector and (d) FID-methanator.

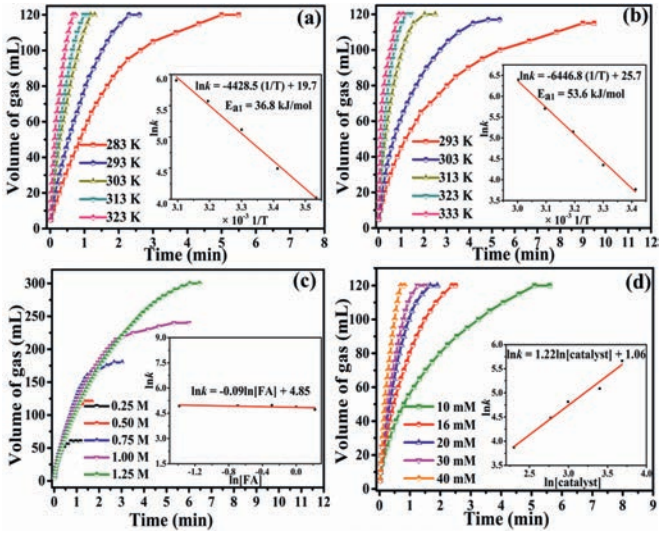

Fig. 4. Volume of generated gas *versus* time for FDR over (a) PdIr/KIT-6-NH_2 and (b) Pd/KIT-6-NH_2 at different temperatures, and volume of generated gas versus time for FDR over PdIr/KIT-6-NH_2 with (c) different FA concentrations and (d) catalyst concentrations (inset: the corresponding kinetic parameters).

sibly attributed to the change of the electronic structure after Pd alloyed with Ir.

The catalytic performances of PdIr/KIT-6-NH_2 and comparative samples were investigated for H_2 generation at 303 K. As shown in Figs. 3a and b, the Pd_6Ir_4-KIT-6-NH_2 catalyst display the best catalytic performance for FA dehydrogenation among a series of samples with different Pd/Ir molar ratios, providing a high TOF value of 3533 h^{-1} (measured by the total metal content of Pd and Ir, at a FA conversion rate of 20%), which is one of the highest values for heterogeneous hydrogen so far (Table S4 in Supporting information). In contrast, physically mixed catalysts (PdIr and KIT-6-NH_2) exhibit a lower activity than that of Pd_6Ir_4/KIT-6-NH_2 under identical conditions (Fig. S7 in Supporting information), further indicating the important contribution of the strong interaction between PdIr and KIT-6-NH_2 on the activity of catalyst toward FDR.

Surface grafted amino-groups play an important role in the catalytic activity of PdIr catalysts. We investigated the catalytic activity of PdIr catalysts confined in KIT-6-NH_2 which was functionalized with different organic amines *via* reflux method (Fig. S8 in Supporting information), and the results show that APTES is a good candidate as the amino-groups for FDR. Bare KIT-6-supported PdIr catalyst has almost no activity (Fig. 3b). However, PdIr NPs supported by KIT-6-NH_2 show an enhanced activity, because the amino-groups on the surface of KIT-6-NH_2 can not only serve as the Brønsted basic sites to provide a basic environment around PdIr NPs to promote the dissociation of the O-H bond of HCOOH, but also act as the anchoring sites to achieve the small PdIr NPs with high dispersity to increase the active sites toward FDR. The results of UV-vis confirmed the strong interaction between the -NH_2 groups of KIT-6-NH_2 and the metal ions (Fig. S9 in Supporting information). Compared with Pd_6Ir_4/SBA-NH_2, Pd_6Ir_4/KIT-6-NH_2 shows a higher activity owing to its 3D cubic la3D structure of KIT-6, which is more conducive to mass transfer than that of SBA-15 with 2D hexagonal P6mm structure (Fig. 3b). The gas mixtures generated from FA catalyzed by PdIr-KIT-6-NH_2 were CO_2 and H_2 analyzed by gas chromatography (GC) (Fig. 3c). There were neither CO nor other gas detected (Fig. 3d) from FDR at 303 K, suggesting that the as-prepared PdIr/KIT-6-NH_2 catalyst has a 100% selectivity for FDR. Besides, the activity of the PdIr/KIT-6-NH_2 catalyst is related to the molar ratio of FA/SF (SF is the abbreviation of sodium formate) and the optima value of FA/SF is 1/2. The presence of SF in the solution can significantly accelerate the hydrogen production rate (Fig. S10 in Supporting information). There is almost no gas production from SF alone, suggesting a negligible contribution from direct SF hydrolysis. The PdIr/KIT-6-NH_2 catalyst with a 15 wt% loading of PdIr NPs (Fig. S11 in Supporting information) shows the best activity among the investigated samples with different metal loading, which is close to the designed theoretical values as examined by ICP-AES (Table S2 in Supporting information). We also studied the activity of Pd alloyed with other noble metals (*i.e.*, Rh, Pt, Au, Ag and Ru). As shown in Fig. S12 (Supporting information), Pd_6Ir_4/KIT-6-NH_2 shows the highest catalytic activity.

The kinetic characteristics of FDR were also studied in Fig. 4. It could be found that the catalytic activity of the catalysts is positively correlated with reaction temperature (Figs. 4a and b). The activation energy of FDR over Pd_6Ir_4/KIT-6-NH_2 is 36.8 kJ/mol, which is lower than that of Pd/KIT-6-NH_2 (53.6 kJ/mol) and most of the reported heterogeneous catalysts (Table S4 in Supporting information). The decrease in the activation energy of FDR over PdIr/KIT-6-NH_2 can be attributed to the smaller size of metal NPs (Fig. S13 in Supporting information) and the contribution of PdIr alloy effects. Figs. 4c and d show FDR over the Pd_6Ir_4/KIT-6 catalyst is near to the first-order reaction and zero-order reaction with respect to catalyst concentrations and FA concentrations, respectively.

As shown in Fig. S14 (Supporting information), the H_2 selectivity and productivity over PdIr/KIT-6-NH_2 toward FDR remain unchanged after four runs, but the activity shows a slightly decrease (Fig. S14). After the reusability test, the recovered catalysts were analyzed by XRD and nitrogen adsorption-desorption analyzed, and there is no obvious change in structure of KIT-6 (Figs. S15 and S16 in Supporting information). The small decrease in the activity of PdIr/KIT-6-NH_2 can be attributed to a slight increase in the size of PdIr NPs (Fig. S17 in Supporting information) and a small decrease of amino-groups amounts of KIT-6-NH_2 analyzed by EA (Table S3 in Supporting information).

In summary, PdIr/KIT-6-NH_2 catalyst was prepared, for the first time, with a simple wet chemical method. Compared with PdIr NPs immobilized by SBA-15-NH_2 and bare KIT-6 without amino-groups, the PdIr/KIT-6-NH_2 catalyst displayed the highest catalytic performance toward FDR, achieving an initial TOF value of 3533

h^{-1} and 100% selectivity at ambient temperature. Besides the contribution of electron-rich Pd-Ir alloy NPs with high dispersion and small size, the high catalytic performance can be attributed to the amino-groups of KIT-6-NH_2, which cannot only serve as the anchoring sites to form the ultrafine PdIr NPs and enhance the interaction between PdIr NPs and KIT-6-NH_2 but also act as a proton scavenger to promote the breaking of O-H bond of FA. This work provides an effective and simple method for preparing ultrafine metal NPs confined by porous carrier for various applications.

Declaration of competing interest

The authors declare that they have no known competing financial interests or personal relationships that could have appeared to influence the work reported in this paper.

Acknowledgments

This work was financially supported by the National Natural Science Foundation of China (Nos. 21763012, 22162014) and Scientific Research Foundation of Graduate School of Jiangxi Province (No. YC2020-B067).

Supplementary materials

Supplementary material associated with this article can be found, in the online version, at doi:10.1016/j.cclet.2021.08.033.

References

[1] Y. Zhang, J. Liu, S. Li, et al., EnergyChem 1 (2019) 100021.
[2] W. Hua, H.H. Sun, F. Xu, et al., Rare Met. 39 (2020) 335–351.
[3] A. Zhang, H. Du, Z.H. Lu, Acta Chim. Sin. 79 (2021) 885–902.
[4] J. Zhang, F. Lin, L. Yang, et al., Chin. Chem. Lett. 31 (2020) 2019–2022.
[5] Z.P. Li, Q. Xu, et al., Acc. Chem. Res. 50 (2017) 1449–1458.
[6] Z.J. Zhang, Y.X. Luo, S.W. Liu, et al., J. Mater. Chem. A 7 (2019) 21438–21446.
[7] Q.M. Sun, J.M. Ben, W.J. Chen, et al., Angew. Chem. Int. Ed. 59 (2020) 20183–20191.
[8] Y. Yang, Z.H. Lu, Y. Hu, et al., RSC Adv. 4 (2014) 13749–13752.
[9] X. Cao, J Zhou, S. Li, et al., Rare Met. 39 (2020) 113–130.
[10] L.S. Jose, M.S. Cristina, I. Svetlana, et al., Appl. Catal. B: Environ. 282 (2021) 119615.
[11] Q.Y. Bi, J.D. Lin, Y.M. Liu, et al., Angew. Chem. Int. Ed. 55 (2016) 11849–11853.
[12] M. Farajzadeh, H. Alamgholiloo, F. Nasibipour, et al., Sci. Rep. 10 (2020) 18188.
[13] Y. Luo, W. Nie, Y. Ding, et al., ACS Appl. Energy Mater. 4 (2021) 4945–4954.
[14] Y. Chao, X.F. Guo, B. Shen, et al., J. Mater. Chem. A 6 (2018) 23766–23772.
[15] J. Han, Z.J. Zhang, Z.R. Hao, et al., J. Colloid Interfaces Sci. 587 (2021) 736–742.
[16] K. Mori, S.Y. Masuda, H. Tanaka, et al., Chem. Commun. 53 (2017) 4677–4680.
[17] J.L. Santos, C. Leon, G. Monnier, et al., Int. J. Hydrog. Energy 45 (2020) 23056–23068.
[18] W. Hong, M. Kitta, N. Tsumori, et al., J. Mater. Chem. A 7 (2019) 18835–18839.
[19] Z.Z. Wang, S.P. Liang, X.Y. Meng, et al., Appl. Catal. B: Environ. 291 (2021) 120140.
[20] W. Wang, X. Hong, Q. Yao, et al., J. Mater. Chem. A 8 (2020) 13694–13701.
[21] C.G. Jessica, N.G. Miriam, S.T. David, et al., ACS Sustain. Chem. Eng. 8 (2020) 15030–15043.
[22] T. Wang, J. Du, Y. Sun, et al., Chin. Chem. Lett. 32 (2021) 1186–1190.
[23] Y. Yan, H. Li, Z.H. Lu, et al., Chin. Chem. Lett. 30 (2019) 1153–1156.
[24] J. Cheng, X. Gu, X.L. Sheng, et al., J. Mater. Chem. A 4 (2016) 1887 184.
[25] K. Wang, Q.L. Yao, S.J. Qing, et al., J. Mater. Chem. A 7 (2019) 9903–9911.
[26] I. Choi, H.K. Lee, G.W. Lee, et al., Rare Met. 39 (2020) 767–783.
[27] Z. Pan, Z. Tang, Y. Zhang, et al., Tungsten 2 (2020) 390–402.
[28] Z. Zhang, S. Zhang, Q. Yao, et al., Inorg. Chem. Front. 5 (2018) 370–377.
[29] K. Zhan, P. Liu, J. Dong, et al., Chin. Chem. Lett. 31 (2020) 1630–1634.
[30] J.M. Yan, S.J. Li, S.S. Yi, et al., Adv. Mater. 30 (2018) 1703038.
[31] F.Z. Song, Q.L. Zhu, X.C. Yang, et al., Adv. Energy Mater. 8 (2017) 1701416.
[32] Z.Z. Wang, C.P. Wang, S.J. Mao, J. Mater. Chem. A 7 (2019) 25791–25795.
[33] Q.J. Wang, N. Tsumori, M. Kitta, et al., ACS Catal. 8 (2018) 12041–12045.
[34] X.J. Gu, Z.H. Lu, H.L. Jiang, et al., J. Am. Chem. Soc. 133 (2011) 11822–11825.
[35] X. Li, A.E. Surkus, J. Rabeah, et al., Angew. Chem. Int. Ed. 59 (2020) 15849–15854.
[36] A.B. Redondo, F.L. Morel, M. Ranocchiari, et al., ACS Catal. 5 (2015) 7099–7103.
[37] G.D. Feng, J.Y. Wang, M. Boronat, et al., J. Am. Chem. Soc. 140 (2018) 4770–4773.
[38] Y.D. Zou, B.T. Huang, L.H. Cao, et al., Adv. Mater. 33 (2020) 2005215.
[39] J. Liang, Z.B. Liang, R.Q. Zou, et al., Adv. Mater. 29 (2017) 1701139.
[40] S. Masuda, K. Mori, Y. Futamura, et al., ACS Catal. 8 (2018) 2277–2285.
[41] M. Huang, Q. Yao, G. Feng, et al., Inorg. Chem. 59 (2020) 5781–5790.
[42] K. Koh, M. Jeon, C.W. Yoon, et al., J. Mater. Chem. A 5 (2017) 16150–16161.
[43] Y.X. Luo, Q.F. Yang, W.D. Nie, et al., ACS Appl. Mater. Interfaces 12 (2020) 8082–8090.
[44] W.D. Nie, Y.X. Luo, Q.F. Yang, et al., Inorg. Chem. Front. 7 (2020) 709–717.
[45] S.P. Wang, S.H. Hou, C. Wu, et al., Chin. Chem. Lett. 30 (2019) 398–402.